Precision Measurement of the Lamb Shift in Muonium

B. Ohayon,[1] G. Janka,[1] I. Cortinovis,[1] Z. Burkley,[1] L. de Sousa Borges,[1] E. Depero,[1] A. Golovizin,[2] X. Ni,[3]
Z. Salman,[3] A. Suter,[3] C. Vigo,[1] T. Prokscha,[3] and P. Crivelli[1,*]

(Mu-MASS Collaboration)

[1]*Institute for Particle Physics and Astrophysics, ETH Zürich, CH-8093 Zürich, Switzerland*
[2]*P.N. Lebedev Physical Institute, 53 Leninsky prospekt., Moscow 119991, Russia*
[3]*Laboratory for Muon Spin Spectroscopy, Paul Scherrer Institute, CH-5232 Villigen PSI, Switzerland*

We report a new measurement of the $n = 2$ Lamb shift in Muonium. Our result of $1047.2(2.3)_{\text{stat}}(1.1)_{\text{syst}}$ MHz comprises an order of magnitude improvement upon the previous best measurement. This value matches the theoretical calculation within 1 standard deviation allowing us to set limits on Lorentz and CPT violation in the muonic sector, as well as on new physics coupled to muons and electrons which could provide an explanation of the muon $g - 2$ anomaly.

The classical Lamb shift (LS) is the difference between the $2S_{1/2}$ and $2P_{1/2}$ levels of a hydrogenic atom. It stems in the most part from the so called electron self-energy, i.e., the possibility for the orbiting particle to emit and reabsorb a virtual photon [1]. This effect is not accounted for by the Dirac theory. Following the clear identification of the LS in hydrogen by Lamb and Retherford [2], Bethe completed the first successful calculation of the interaction of an electron with the radiation field [3], finding agreement with the experimental result. The discrepancy between the then-prevailing theory and measurements of the LS, together with that of the electron anomalous moment [4], had found unambiguous evidence for what was at the time new physics. These findings led to the development of modern quantum electrodynamics (QED).

In hydrogen, the increasing precision in LS measurements, as well as more advanced theoretical calculations, have made their comparison susceptible to the proton charge distribution. Various discrepancies in the proton charge radius determination have appeared already in the 1980s [5]. They peaked when another LS measurement, that of muonic hydrogen [6], returned a significantly smaller radius than the accepted one. This is the so-called proton radius puzzle [7], with recent measurements arguably nearing its resolution [8–10]. This saga embodies the fact that when dealing with measurements involving hadronic particles such as protons, at a certain precision we learn more about their internal structure than about the consistency of QED.

In leptonic systems such as muonium (M), the bound state of a positive muon and an electron; and positronium, made of an electron and a positron; hadronic effects are entering only as loop corrections, and there are no finite-size contributions. Precision spectroscopy of such exotic atoms offers a clean arrow pointing at bound-state QED tests and an excellent probe for numerous scenarios beyond the standard model. These include Lorentz or CPT violations [11], new muonic forces [12], dark sectors [13], the effect of gravity on antimatter via the gravitational redshift [14] and to search for highly singular neutrinolike forces [15]. However, despite their simplicity, these systems exhibit unique experimental challenges.

Positronium's very short lifetime due to annihilation results in broad resonances and limits the available statistics. Moreover, being the lightest known atom, positronium travels at high velocities, even at room temperature. Nevertheless, the positronium $n = 2$ fine structure was measured recently by microwave spectroscopy with sub MHz precision [16]. Interestingly, this result differs by 4.5σ from the theoretical prediction and warrants further studies [17].

With a longer lifetime of 2.2 μs limited by the muon decay, and a larger mass, M constitutes a promising system for spectroscopic measurements [18,19].

Previous experiments measuring the LS in M relied on a degrader to reduce the beam energy, creating a highly diffuse M distribution [20]. This resulted in low statistics and caused a large muon-related background. Nevertheless, the LS in M was measured to be 1070^{+12}_{-15} MHz at TRIUMF [21], and 1042^{+21}_{-23} MHz at LAMPF [22]. The main limitation for both measurements was the lack of a high quality, low energy, positive muon beam. Such a beam is available today at the low energy muon (LEM) beam line at the Paul Scherrer Institute (PSI). LEM is a unique beam line, used
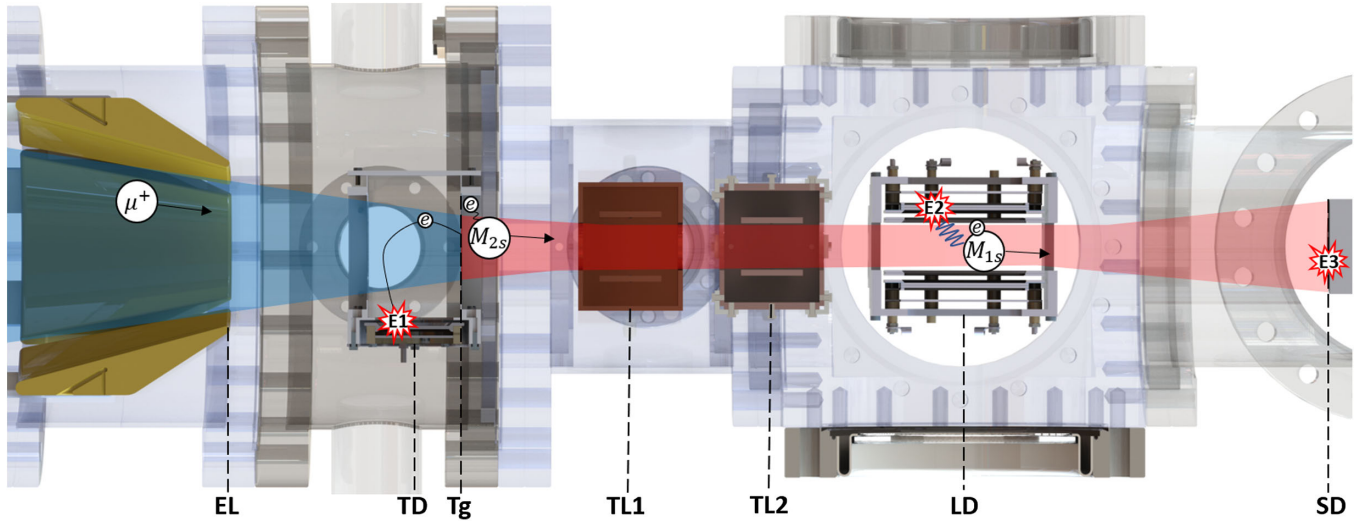
FIG. 1. Main elements of the experimental system. Conical electrostatic lens (EL), tagging detector (TD), carbon foil target (Tg), transmission line (TL), Lyman-alpha detector (LD), stop detector (SD). The normalization signal is given by the coincidence between an event in TD (E1) and SD (E3) within the expected time of flight, while a valid event includes also a reading in LD (E2).

primarily for muon spin rotation (μSR) experiments [23], which provides a pure μ^+ beam with selectable energy between 1 and 30 keV [24]. Following our demonstration of an intense M_{2S} beam production at the LEM [25], we report here on a precision measurement of the muonium Lamb shift comprising an order of magnitude improvement.

In our experiment, muons ($\sim 2 \times 10^8$ μ^+/s, momentum 28 MeV/c) from the μE4 beam line [24] are implanted into a neon moderator from which they are reemitted as epithermal muons with an energy of roughly 20 eV. These are accelerated by a dc voltage of 7.5 kV and transported electrostatically. An $E \times B$ filter selects only muons while rejecting other particles such as protons and neon atoms from the moderator [26]. The beam is guided to our apparatus depicted in Fig. 1, where a segmented conical electrostatic lens [27] focuses it onto a 10 nm-thick grounded carbon foil target. The foil serves a double purpose: producing M, and tagging the incoming muons.

When passing the foil, a particle has a high probability of backscattering an electron [28]. This electron is guided by an electric field and collected on a microchannel plate (MCP) detector, thus tagging the incoming muons. We measured the tagging efficiency, through coincidence measurement with another tagging detector, to be 67 (3)%. The measured rate at the tagging detector was 13–15 kHz, out of which we estimate that 9.3(4) kHz is the tagged muon rate at the foil, and the rest is beam-related background. For an incident energy of 7.5 keV, 43 (2)% of the muons that traversed the foil produce muonium, out of which 11(4)% are in long-lived excited states [25]. In the absence of electromagnetic fields, the $2S$ M radiative lifetime is 0.12 s, which far exceeds the muon lifetime and any other timescale in this experiment.

Within the detection region, the beam encounters a static electric field of 250 V/cm, which mixes the $2S$ with the short-lived $2P$ levels and relaxes them within few nanoseconds to the ground state, emitting a Lyman-alpha photon at 122 nm. This process is referred to as *quenching*. These photons are detected by two coated MCPs placed around the quenching region. By simulating the field within this region, combined with the M position and energy distribution, we estimate that the total quenching and collection efficiency is around 40%.

Microwave (MW) radiation, resonant with one of the $^2S_{1/2} - {}^2P_{1/2}$ transitions (see Fig. 2), reduces the Lyman-alpha signal by depopulating M_{2S} atoms before they reach the detection region. By scanning the MW around the different transitions, we measure the resonance shape from which we determine the line center and finally deduce the LS defined as the difference between the centroid $^2S_{1/2} - {}^2P_{1/2}$ binding energies averaged over all hyperfine levels [as shown in Fig. 2 or see also Eq. (1) of Ref. [29]].

For this purpose, we placed two balanced dual transmission lines (TLs) in the beam path. The design is similar to Ref. [30], in which a pair of parallel electrodes is driven
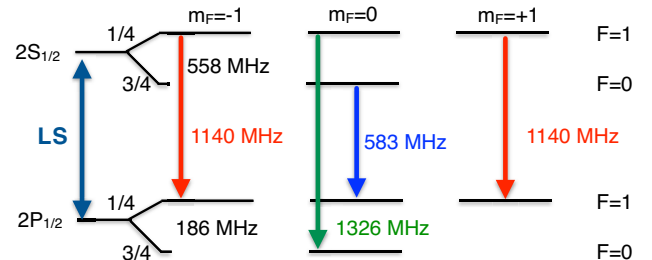

FIG. 2. Scheme of the M $2S_{1/2} - 2P_{1/2}$ energy levels.

180° out of phase. In this configuration, M traveling in the center of the TL flies through a virtual ground plane which ensures that the field is linearly polarized perpendicular to the atomic beam.

At the end of the setup a position sensitive MCP detector acts as a beam monitor. This MCP is also used to measure the muon time of flight (TOF) and to trigger the data acquisition when a signal (events E3 in Fig. 1) is detected in coincidence with the tagging detector within 10 μs. We select TOFs that are compatible with those expected for muons at the given beam energy, taking into account losses in the foil. The coincidence rate (events E1 and E3 in Fig. 1) was $R_D = 105$ Hz and reduced slowly to 95 Hz within four days of continuous running due to aging of the neon moderator. R_D is the sum of the muons, M, and a negligible background rate and is used as a normalization. Our signal as a function of frequency is defined as $S(f) = R_T(f)/R_D(f)$, with R_T the rate of triple coincidences (events E1, E2, and E3 in Fig. 1). This signal corresponds to the probability of creating and detecting photons from quenched M in long-lived excited states per tagged muon that has reached SD.

To reduce the background, and minimize line pulling, we drive 86(5)% of the $2S_{F=0}$ population to the ground state by applying a frequency of 583 MHz to TL2, while scanning the two $2S_{F=1}$ resonances in the range 900–1400 MHz with TL1. Data taking took place for 48 h, continuously, and constituted of cycles in which 9 frequency points were measured (each point for 20 min), as well as one with TL1 off.

The total MW power was measured continuously outside the vacuum system. To determine the average power seen by the atoms in the TL center we measured the frequency-dependent power loss and calibrated accordingly. We then applied a correction to the data points in order to mimic data taken with a constant power of 29 W in the TL center. The corrected signal is denoted $S_c(f)$ and is plotted in Fig. 3. Its main features are two overlapping resonances corresponding to the two allowed transitions from the $2S_{F=1}$ hyperfine level.

To determine the line center from $S_c(f)$ we fit the data with line shapes obtained from a Monte Carlo simulation based on GEANT4 modeling of the LEM beam line [31] validated with data [32]. The same selection criteria applied to the experimental data are used for the simulated events. Because of the linear polarization of the MW field, a 2-level model is sufficient to calculate the transition probability, and so we simulate by solving the relevant Bloch equations [33]. The density matrix equations are integrated numerically for each atom's trajectory within the simulated time-dependent fields of the TLs. Since we do not employ the rotating wave approximation, the Bloch-Siegert shift is included in our line shape model. The MW phase is chosen randomly for each atom before entering the TLs so that it is averaged out.

The transitions of interest for our measurement are the $2S_{F=0} - 2P_{1/2,F=1}$ at 583 MHz, $2S_{F=1} - 2P_{1/2,F=1}$ at
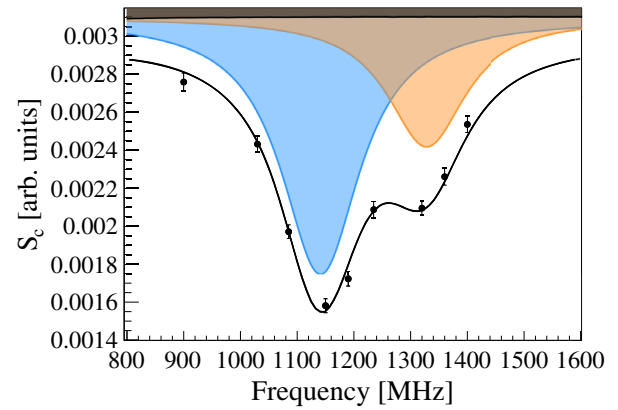

FIG. 3. Measured resonance with the best line shape fit to the data (solid line). The MW off data point (not shown in the figure) lies at $(2.96 \pm 0.05) \times 10^{-3}$. The filled areas correspond to the individual contributions as described in the main text.

1140 MHz and the $2S_{F=1} - 2P_{1/2,F=0}$ at 1326 MHz (see Fig. 2). The fitting procedure is done by χ^2 minimization using the Minuit library within the ROOT package [34]. The free parameters returned by the fit are the resonance position 1139.9(2.3) MHz (the $2P_{1/2}$ hyperfine splitting is fixed), an overall magnitude of $31.5(10) \times 10^{-4}$, and a frequency-independent background parameter of $5.9(6) \times 10^{-4}$. The fit has a reduced chi square of 1.16 for 7 d.o.f.

The compact nature of our setup, coupled with the high velocity of the beam, which travels on average 70 ns between the foil and our detection system, makes us susceptible to contamination from other long-lived excited states which are populated by the beam-foil interaction and have transitions within our frequency range. The relevant transitions are between $4S - 4P_{3/2}$ around 1240 MHz [35]. From the frequency-independent background, we estimate the maximal contribution of all excited states to be 17%. Using the scaling factor of $1/n^3$ as in Ref. [36], we get a contribution of 5% for $4S$ states. This is validated by keeping the magnitude of the $4S$ contribution as a free-fit parameter, which returns a value compatible with zero. A dedicated measurement of hydrogen LS using protons available in the same beam line supports our limit. Therefore, to estimate this contribution, we fit the data adding 5% $4S$ fraction and conservatively use the full 1.0 MHz offset as the uncertainty to the line center.

To estimate the influence of the simulation input parameters on the resonance position, we scan them around their uncertainty and repeat the analysis. The ones that were found to give the largest contributions are (1) The MW field intensity with an uncertainty of 6% originating from the absolute calibration of the power meter (3%) and from the mechanical tolerances in the TL construction (5%). The estimated systematic uncertainty is 0.04 MHz arising from the uncertainty in the ac Stark shift. (2) The M velocity distribution determined by the muon scattering in the C

TABLE I. Central values and uncertainty contributions in MHz.

	Central value	Uncertainty
Fitting	1139.9	2.3
4S contribution		<1.0
MW-beam alignment		<0.32
MW field intensity		<0.04
M velocity distribution		<0.01
ac Stark $2P_{3/2}$	+0.26	<0.02
2nd-order Doppler	+0.06	<0.01
Earth's field		<0.05
Quantum interference		<0.04
$2S_{F=1} - 2P_{1/2,F=1}$	1140.2	2.5
Hyperfine	−93.0	0.0
Lamb shift	1047.2	2.5
Theoretical value [13]	1047.284	0.002

foil. As demonstrated with previous measurements, our simulation reproduces the TOF distribution very accurately with an uncertainty on the mean energy loss of a few % [32]. This corresponds to a mean M energy of $E_M = 5.7(2)$ keV resulting in an uncertainty of 0.01 MHz. (3) A misalignment of the TL axis with respect to the beam could lead to a residual first order Doppler shift. Taking into account the mechanical tolerances in the TL construction, we set an upper limit on the misalignment angle of 30 mrad which would amount to a 0.32 MHz shift. The above contributions are summarized in Table I.

Other effects not included in the simulation can shift the central value. The main one is an overestimation of the ac Stark shift as we did not include the $2P_{3/2}$ states in the Bloch equations. Nevertheless, this effect is well understood theoretically [37] and validated experimentally [38], so that it can be corrected by multiplying it with a factor 0.64 resulting in +0.26(2) MHz. In Table I, we give the magnitude of several smaller systematic effects, namely, the 2nd-order Doppler, motional Stark shift from the Earth's magnetic field, and quantum interference shift from the presence of M_{3S} [39].

Adding all corrections, the determined frequency of the $2S_{F=1} - 2P_{1/2,F=1}$ transition is $1140.2(2.3)_{\text{stat}}(1.1)_{\text{syst}}$ MHz and the corresponding LS is 1047.2(2.5) MHz, where we added the statistical and systematic uncertainties in quadrature. Our result is within 1 standard deviation from the theoretical value quoted in the literature of 1047.5(3) MHz [22] (to be updated [29]) and a calculation based on effective field theory giving 1047.284(2) MHz [13,40].

Since our result is in agreement with the theoretical calculations, we can use it to place stringent limits on new physics scenarios. Here we focus on possible Lorentz and CPT violation effects, and new bosons interacting with muons and electrons. The M Lamb shift is sensitive to two of the isotropic nonrelativistic effective coefficients for Lorentz and CPT violation [11]: namely, $\overset{\circ}{a}_4^{\text{NR}}$ and $\overset{\circ}{c}_4^{\text{NR}}$.

TABLE II. Single constraints from the Lamb shift measurement on isotropic nonrelativistic coefficients for Lorentz and CPT violation.

Coefficient	Constraint
$|\overset{\circ}{a}_4^{\text{NR}}|$	$<1.7 \times 10^5$ GeV^{-3}
$|\overset{\circ}{c}_4^{\text{NR}}|$	$<1.7 \times 10^5$ GeV^{-3}

Taking conservatively 2σ, we can set a bound on the linear combination,

$$|\overset{\circ}{a}_4^{\text{NR}} + \overset{\circ}{c}_4^{\text{NR}}| < 1.7 \times 10^5 \text{ GeV}^{-3}, \tag{1}$$

which translates into Table II, when considering only one coefficient at a time to be nonzero. These bounds are of the same order as the current ones obtained from the measurement of the 1S-2S transition in M [41], and improve by an order of magnitude the previous bounds from the M Lamb shift.

A new scalar or a new vector gauge boson could provide an explanation of the muon $g - 2$ anomaly [42–44]. If this particle is carrying a dark force between electrons and muons, then M spectroscopy offers the possibility to search for it [13]. For the scalar case, one has a Yukawa-like attractive potential of the form (see, e.g., Ref. [45]):

$$V_{ss}(\vec{r}) = -g_e^s g_\mu^s \frac{e^{-m_s r}}{4\pi r}, \tag{2}$$

where m_s is the scalar boson mass and g_e^s, g_μ^s are the coupling strengths to electrons and antimuons, respectively. For small coupling strengths, the effect of such a potential can be calculated by applying perturbation theory. The vector potential can be found in Ref. [45]. In Fig. 4, we
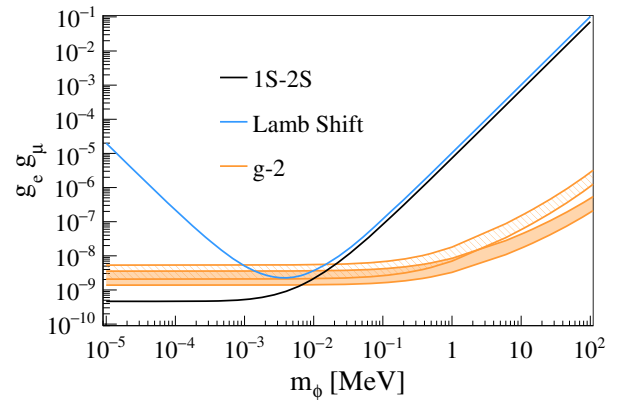

FIG. 4. Constraints from M spectroscopy on g_e^s, g_μ^s as a function of the scalar or vector mass. The solid black line is the constraint from the M 1S-2S measurement [41] while the blue line is from the LS measurement presented here. The orange band represents the region suggested by the $g - 2$ muon anomaly considering the lower bound from the measurement of the electron gyromagnetic factor for the scalar case, while the hatched region is for the vector one.

present the sensitivity of Muonium spectroscopy to new physics. The constraints on g_e^s, g_μ^s as a function of the scalar or vector mass, which are nearly identical in the mass range considered here, are compared to the region favored by the $g - 2$ muon anomaly [46], considering the bounds from the electron gyromagnetic factor [47–49]. We do not present results from experiments at the intensity frontier since those can be argued to be model dependent. An example is the NA64 experiment placing stringent bounds on new bosons with the assumption that those would decay invisibly [50]. The combination of the LS and $1S$-$2S$ M measurements provides the most stringent laboratory constraint excluding that a new scalar or vector boson with a mass < 10 keV could contribute to the muon $g - 2$ anomaly.

To conclude, we report a new measurement of the $n = 2$ Lamb shift in muonium. Our result of $1047.2(2.3)_{\text{stat}}(1.1)_{\text{syst}}$ MHz comprises an order of magnitude of improvement upon the best previously determined value. As it agrees with the theoretical value within 1 standard deviation, we have set limits on Lorentz and CPT violation in the muonic sector, as well as new physics coupled to muons and electrons.

A major increase in statistics could be obtained if beam scattering by the foil would be considerably reduced. Graphene foils [51] are 5–10 times thinner than our currently used foil. As the scattering half angle is proportional to the foil thickness [52], our statistics could be increased by a factor 15–25. Therefore, the main systematic uncertainty, originating from a possible contamination of the M_{2S} beam of higher excited states, would become comparable with the statistical one. These states could be suppressed by introducing a weak quenching field between Tg and TLs [53]. Beam misalignment could be compensated by periodically reversing the MW direction, thus reducing the associated uncertainty by more than an order of magnitude [35]. These straightforward improvements would increase the precision to ~ 300 kHz level extending significantly the reach of muonium spectroscopy to search for new physics.

The realization of the high intensity muon beam (HiMB) at PSI [54] would open the way to push the accuracy of this experiment to its ultimate limit of few tens of kHz. Combined with other ongoing M spectroscopy experiments [19,55,56], one would probe the very interesting region of parameter space for a new scalar or vector boson with $m_\phi > 300$ keV where astrophysical bounds do not apply [57].

*Corresponding author.
crivelli@phys.ethz.ch

[1] V. F. Weisskopf, Phys. Rev. **56**, 72 (1939).
[2] W. E. Lamb and R. C. Retherford, Phys. Rev. **72**, 241 (1947).
[3] H. A. Bethe, Phys. Rev. **72**, 339 (1947).
[4] J. Schwinger, Phys. Rev. **73**, 416 (1948).
[5] H. Grotch, Phys. Scr. T **T21**, 86 (1988).
[6] R. Pohl *et al.*, Nature (London) **466**, 213 (2010).
[7] R. Pohl, R. Gilman, G. A. Miller, and K. Pachucki, Annu. Rev. Nucl. Part. Sci. **63**, 175 (2013).
[8] W. Ubachs, Science **370**, 1033 (2020).
[9] J.-P. Karr, D. Marchand, and E. Voutier, Nat. Rev. Phys. **2**, 601 (2020).
[10] H. Gao and M. Vanderhaeghen, arXiv:2105.00571.
[11] A. H. Gomes, V. A. Kostelecký, and A. J. Vargas, Phys. Rev. D **90**, 076009 (2014).
[12] S. G. Karshenboim, D. McKeen, and M. Pospelov, Phys. Rev. D **90**, 073004 (2014); **90**, 079905(E) (2014).
[13] C. Frugiuele, J. Pérez-Ríos, and C. Peset, Phys. Rev. D **100**, 015010 (2019).
[14] S. G. Karshenboim, Astron. Lett. **35**, 663 (2009).
[15] Y. V. Stadnik, Phys. Rev. Lett. **120**, 223202 (2018).
[16] L. Gurung, T. J. Babij, S. D. Hogan, and D. B. Cassidy, Phys. Rev. Lett. **125**, 073002 (2020).
[17] L. Gurung, T. J. Babij, J. Pérez-Ríos, S. D. Hogan, and D. B. Cassidy, Phys. Rev. A **103**, 042805 (2021).
[18] K. P. Jungmann, J. Phys. Soc. Jpn. **85**, 091004 (2016).
[19] B. Ohayon, Z. Burkley, and P. Crivelli, SciPost Phys. Proc. 29 (2021).
[20] P. R. Bolton, A. Badertscher, P. O. Egan, C. J. Gardner, M. Gladisch, V. W. Hughes, D. C. Lu, M. Ritter, P. A. Souder, J. Vetter, G. zu Putlitz, M. Eckhause, and J. Kane, Phys. Rev. Lett. **47**, 1441 (1981).
[21] C. J. Oram, J. M. Bailey, P. W. Schmor, C. A. Fry, R. F. Kiefl, J. B. Warren, G. M. Marshall, and A. Olin, Phys. Rev. Lett. **52**, 910 (1984).
[22] K. Woodle *et al.*, Phys. Rev. A **41**, 93 (1990).
[23] E. Morenzoni, H. Glückler, T. Prokscha, H. Weber, E. Forgan, T. Jackson, H. Luetkens, C. Niedermayer, M. Pleines, M. Birke, A. Hofer, J. Litterst, T. Riseman, and G. Schatz, Physica (Amsterdam) **289B–290B**, 653 (2000).
[24] T. Prokscha, E. Morenzoni, K. Deiters, F. Foroughi, D. George, R. Kobler, A. Suter, and V. Vrankovic, Nucl. Instrum. Methods Phys. Res., Sect. A **595**, 317 (2008).
[25] G. Janka *et al.*, Eur. Phys. J. C **80**, 804 (2020).
[26] Z. Salman, T. Prokscha, P. Keller, E. Morenzoni, H. Saadaoui, K. Sedlak, T. Shiroka, S. Sidorov, A. Suter, V. Vrankovic, and H.-P. Weber, Phys. Procedia **30**, 55 (2012).
[27] R. Xiao, E. Morenzoni, Z. Salman, B.-J. Ye, and T. Prokscha, Nucl. Sci. Technol. **28**, 29 (2017).
[28] F. Allegrini, R. W. Ebert, and H. O. Funsten, J. Geophys. Res. **121**, 3931 (2016).
[29] V. A. Yerokhin, K. Pachucki, and V. Patkóš, Ann. Phys. (Berlin) **531**, 1800324 (2019).

[30] S. R. Lundeen and F. M. Pipkin, Metrologia **22**, 9 (1986).

[31] K. Sedlak, R. Scheuermann, T. Shiroka, A. Stoykov, A. Raselli, and A. Amato, Phys. Procedia **30**, 61 (2012).

[32] K. S. Khaw, A. Antognini, P. Crivelli, K. Kirch, E. Morenzoni, Z. Salman, A. Suter, and T. Prokscha, J. Instrum. **10**, P10025 (2015).

[33] M. Haas, U. D. Jentschura, C. H. Keitel, N. Kolachevsky, M. Herrmann, P. Fendel, M. Fischer, T. Udem, R. Holzwarth, T. W. Hänsch, M. O. Scully, and G. S. Agarwal, Phys. Rev. A **73**, 052501 (2006).

[34] R. Brun and F. Rademakers, Nucl. Instrum. Methods Phys. Res., Sect. A **389**, 81 (1997).

[35] D. A. Andrews and G. Newton, Phys. Rev. Lett. **37**, 1254 (1976).

[36] G. Newton, D. Andrews, and P. Unsworth, Phil. Trans. R. Soc. A **290**, 373 (1979).

[37] D. A. Andrews and G. Newton, J. Phys. B **9**, 1453 (1976).

[38] D. A. Andrews and G. Newton, J. Phys. B **8**, 1415 (1975).

[39] A. Marsman, M. Horbatsch, and E. A. Hessels, Phys. Rev. A **96**, 062111 (2017).

[40] C. Peset and A. Pineda, Eur. Phys. J. A **51**, 156 (2015).

[41] V. Meyer *et al.*, Phys. Rev. Lett. **84**, 1136 (2000).

[42] F. Jegerlehner and A. Nyffeler, Phys. Rep. **477**, 1 (2009).

[43] C. Delaunay, B. Ohayon, and Y. Soreq, Phys. Rev. Lett. **127**, 251801 (2021).

[44] R. Balkin, C. Delaunay, M. Geller, E. Kajomovitz, G. Perez, Y. Shpilman, and Y. Soreq, Phys. Rev. D **104**, 053009 (2021).

[45] P. Fadeev, Y. V. Stadnik, F. Ficek, M. G. Kozlov, V. V. Flambaum, and D. Budker, Phys. Rev. A **99**, 022113 (2019).

[46] B. Abi *et al.* (Muon g-2 Collaboration), Phys. Rev. Lett. **126**, 141801 (2021).

[47] D. Hanneke, S. Fogwell, and G. Gabrielse, Phys. Rev. Lett. **100**, 120801 (2008).

[48] R. H. Parker, C. Yu, W. Zhong, B. Estey, and H. Müller, Science **360**, 191 (2018).

[49] L. Morel, Z. Yao, P. Cladé, and S. Guellati-Khélifa, Nature (London) **588**, 61 (2020).

[50] Y. M. Andreev *et al.* (NA64 Collaboration), Phys. Rev. Lett. **126**, 211802 (2021).

[51] F. Allegrini, R. W. Ebert, S. A. Fuselier, G. Nicolaou, P. V. Bedworth, S. W. Sinton, and K. J. Trattner, Opt. Eng. (Bellingham, Wash.) **53**, 024101 (2014).

[52] A. D. Vira, P. A. Fernandes, H. O. Funsten, S. K. Morley, H. Yamaguchi, F. Liu, and N. A. Moody, Rev. Sci. Instrum. **91**, 033302 (2020).

[53] N. Bezginov, T. Valdez, M. Horbatsch, A. Marsman, A. C. Vutha, and E. A. Hessels, Science **365**, 1007 (2019).

[54] K. Kirch, Slow muons and muonium, in *CPT and Lorentz Symmetry* (World Scientific, Singapore, 2017), pp. 53–56.

[55] P. Crivelli, Hyperfine Interact. **239**, 49 (2018).

[56] S. Kanda, Phys. Lett. B **815**, 136154 (2021).

[57] E. Hardy and R. Lasenby, J. High Energy Phys. 02 (2017) 33.